# Solutions Manual and Online Exercises for Passive Seismic Monitoring of Induced Seismicity

Fundamental Principles and Application to Energy Technologies

DAVID W.S. EATON

# Contents

# Preface

The manual provides solutions to the problems that are found at the end of each chapter in the accompanying textbook, as well as a set of computer exercises. The problems are intended to encourage students to achieve a deeper, quantitative grasp of the key concepts in the book, rather than only a superficial understanding from reading alone. For some of the problems, the solutions will require a synthesis of material from earlier chapters in the book. Symbols, Equation and Figure numbering used in this manual are the same as those in the book. For ease of reference, the problems are repeated in the manual and are set in italic font.

Computer exercises are provided for some chapters, along with sample Matlab programs and datasets. Matlab is a high-performance language for technical computing; many excellent introductory books and online articles are available to provide tutorials. The focus of the software is practical, with the aim of demonstrating concepts outlined in the book by performing simple calculations or processing sample datasets on a single-user desktop or laptop system. The software has been tested with Matlab version R2012a, although newer versions of Matlab may also work.

# 1 Chapter 1

## 1.1 Problem 1

*Evaluate the following.*

a) *What is Poisson's ratio for a Poisson solid (i.e. a material with $\lambda = \mu$)?*

Using the formula in Table 1.1, $\nu = 0.25$ in the case where $\lambda = \mu$.

b) *Given Young's modulus $E = 8 \times 10^{10}$ Pa and Poisson's ratio $\nu = 0.28$, determine $K, \lambda$ and $\mu$.*

Using formulae in Table 1.1, $K = 6.1 \times 10^{10}$ Pa, $\lambda = 4.0 \times 10^{10}$ Pa and $\mu = 3.1 \times 10^{10}$ Pa.

c) *Assuming that these parameters correspond to an isotropic elastic solid, write the stiffness matrix in Voigt form (as in Equation 1.11).*

In Voigt form, the symmetric stiffness matrix may be written in units of $10^{10}$ Pa as:

$$\begin{bmatrix} 10.2 & 4.0 & 4.0 & 0 & 0 & 0 \\ & 10.2 & 4.0 & 0 & 0 & 0 \\ & & 10.2 & 0 & 0 & 0 \\ & & & 3.1 & 0 & 0 \\ & & & & 3.1 & 0 \\ & & & & & 3.1 \end{bmatrix}$$

d) *How would the stiffness matrix change after applying an arbitrary rotation?*

No change would occur, as the stiffness matrix is isotropic.

e) *What is the value of the elastic stiffness $c_{1111}$?*

$c_{1111} = \lambda + 2\mu = 10.2 \times 10^{10}$ Pa.

## 1.2 Problem 2

*Consider a hypothetical granitic material that can be approximated as a 6-phase assemblage of minerals, as tabulated below.*

| Mineral | Volume Fraction (%) | $K$ [GPa] | $\mu$ [GPa] |
|---|---|---|---|
| quartz | 30 | 36 | 42 |
| orthoclase | 30 | 40 | 24 |
| plagioclase | 25 | 65 | 39 |
| muscovite | 5 | 45 | 27 |
| biotite | 5 | 40 | 24 |
| amphibole | 5 | 100 | 60 |

*Determine the bulk modulus, $K$, of the polycrystalline aggregate using the following methods.*

a) *Voigt averaging.*

Using Equation 1.22, $K_V = 48.3$ GPa.

b) *Reuss averaging.*

Using Equation 1.23, $K_R = 44.4$ GPa

c) *Voigt-Reuss-Hill (VRH) averaging.*

The Voigt-Reuss-Hill average is simply the average of $K_V$ and $K_R$, or 46.3 GPa.

d) *Hashin-Shtrikman extremal bounds (calculate upper and lower bounds).*

Using Equations 1.24 to 1.26 with $K_0 = 36$ GPa and $\mu_0 = 42$ GPa, $K_{HS}^{-} = 46.2$ GPa. Quartz is used for the $0th$ phase as it has the smallest value of $K$.

Using Equations 1.27 to 1.29 with $K_N = 100$ GPa and $\mu_N = 60$ GPa, $K_{HS}^{+} =$ 46.5 GPa. Amphibole is used for the $Nth$ phase ($N = 5$) as it has the largest value of $K$.

## 1.3 Problem 3

*In Voigt notation, the stiffness matrix of an isotropic solid can be written in terms of Lamé parameters as*

$$\tilde{\mathbf{C}} = \begin{bmatrix} \lambda+2\mu & \lambda & \lambda & 0 & 0 & 0 \\ \lambda & \lambda+2\mu & \lambda & 0 & 0 & 0 \\ \lambda & \lambda & \lambda+2\mu & 0 & 0 & 0 \\ 0 & 0 & 0 & \mu & 0 & 0 \\ 0 & 0 & 0 & 0 & \mu & 0 \\ 0 & 0 & 0 & 0 & 0 & \mu \end{bmatrix} .$$

*Suppose that the elastic properties of an unfractured granite can be approximated by the following stiffness matrix:*

$$\tilde{\mathbf{C}} = \begin{bmatrix} 80 & 20 & 20 & 0 & 0 & 0 \\ 20 & 80 & 20 & 0 & 0 & 0 \\ 20 & 20 & 80 & 0 & 0 & 0 \\ 0 & 0 & 0 & 30 & 0 & 0 \\ 0 & 0 & 0 & 0 & 30 & 0 \\ 0 & 0 & 0 & 0 & 0 & 30 \end{bmatrix} [\mathrm{GPa}] .$$

*Now, suppose that the granite contains fractures with a transverse fracture compliance* $Z_T = 3.0 \times 10^{-12}$ $Pa^{-1}$*. Determine the stiffness matrix for the case of:*

a) *penny-shaped fractures that are well drained (Equation 1.46);*
b) *smooth fractures filled with an incompressible fluid.*

a) To solve this problem, first use $\lambda = 20$ GPa and $\mu = 30$ GPa to determine Poisson's ratio, $\nu = 0.2$. Using this, Equation 1.46 yields $Z_N = 2.7 \times 10^{-12}$ Pa$^{-1}$. Next, determine the compliance matrix of the unfractured rockmass by computing the inverse of the stiffness matrix (this can be done numerically). Then, form the compliance perturbation matrix using Equation 1.45. The compliance of the fractured rock is given by Equation 1.44. Taking the inverse yields the stiffness matrix of the fractured rockmass (in units of GPa):

$$\begin{bmatrix} 65.7 & 16.4 & 16.4 & 0 & 0 & 0 \\ & 79.1 & 19.1 & 0 & 0 & 0 \\ & & 79.1 & 0 & 0 & 0 \\ & & & 30 & 0 & 0 \\ & & & & 27.5 & 0 \\ & & & & & 27.5 \end{bmatrix}$$

b) In this case, $Z_N = 0$. The stiffness matrix of the fractured rock mass is the same as the unfractured rock mass, except that $C_{55} = C_{66} = 27.5$ GPa.

## 1.4 Problem 4

*Consider a binary sequence of shale and coal layers, where the shale is characterized by Lamé parameters $\lambda$ = 8.0 GPa and $\mu$ = 9.0 GPa, while the coal is characterized by Lamé parameters $\lambda$ = 4.0 GPa and $\mu$ = 2.0 GPa. Using Backus averaging, determine the Voigt matrix for the equivalent TI medium based on the following relative abundances:*

a) *equal-thickness layers of coal and shale;*

b) *coal layers that are 10% of the thickness of shale layers, on average.*

a) To solve this problem, use Equations 1.36 - 1.40. Note that the expected value is simply the arithmetic average for coal and shale. Then fill in the stiffness matrix using Equation 1.20 and the formula below it for $C_{12}$. This yields the following stiffness matrix, in units of GPa.

$$\begin{bmatrix} 16.8 & 5.8 & 4.9 & 0 & 0 & 0 \\ & 16.8 & 4.9 & 0 & 0 & 0 \\ & & 12.2 & 0 & 0 & 0 \\ & & & 3.3 & 0 & 0 \\ & & & & 3.3 & 0 \\ & & & & & 5.5 \end{bmatrix}$$

b) This is the same as in part (a), except that a weighted average is used (10% coal, 90% shale). This yields the following stiffness matrix, in units of GPa.

$$\begin{bmatrix} 24.1 & 7.5 & 6.9 & 0 & 0 & 0 \\ & 24.1 & 6.9 & 0 & 0 & 0 \\ & & 21.2 & 0 & 0 & 0 \\ & & & 6.7 & 0 & 0 \\ & & & & 6.7 & 0 \\ & & & & & 8.3 \end{bmatrix}$$

## 1.5 Problem 5

*Given the poroelastic parameters in the Table below, use Equations 1.52-1.54 to perform fluid-substitution calculations, based on Gassmann's formula, to determine the saturated bulk modulus and bulk density of a porous rock that is initially saturated with brine and then becomes fully saturated (after fluid substitution) with supercritical $CO_2$.*

| Property | Symbol | Value |
|---|---|---|
| Initial fluid density (brine) | $\rho_{F0}$ | 1230 kg/m$^3$ |
| Substituted fluid density ($CO_2$) | $\rho_{F1}$ | 625 kg/m$^3$ |
| Matrix density | $\rho_M$ | 2650 kg/m$^3$ |
| Matrix bulk modulus | $K_M$ | 38.8 GPa |
| Initial fluid bulk modulus (brine) | $K_{F0}$ | 3.8 GPa |
| Substituted fluid bulk modulus ($CO_2$) | $K_{F1}$ | 0.25 GPa |
| Initial saturated bulk modulus | $K_{S0}$ | 22.0 GPa |
| Porosity | $\phi$ | 18% |

In order to solve this problem, begin by using the quantities in the table with Equation 1.54 to determine the dry frame modulus, $K_D = 16.1$ GPa. With this, all of the quantities on the right hand side of Equation 1.52 are known and the bulk modulus of the saturated medium can be determined, $K_S = 16.5$ GPa. Finally, use Equation 1.53 to determine the density of the saturated medium, $\rho = 2286$ kg/m$^3$.

## 1.6 Problem 6

*Given a pore-pressure gradient of 1.5 $\times 10^5$ Pa/m, a medium permeability of 1 $\times 10^{-14}$ $m^2$ (0.01 Darcy) and viscosity values of $10^{-3}$ Pa-s for fluid 1 (brine) and $10^{-4}$ Pa-s for fluid 2 (a supercritical fluid), determine the following.*

a) *Estimate the fluid velocity using Darcy's Law (Equation 1.63).*

Using Equation 1.63 with the parameters specified above, the fluid velocity is 1.5 $\times 10^{-6}$ m/s for brine and 1.5 $\times 10^{-5}$ m/s for a supercritical fluid, respectively.

b) *For a porosity of 18%, what is the seepage velocity?*

The seepage velocity is 8.3 $\times 10^{-6}$ m/s for brine and 8.3 $\times 10^{-5}$ m/s for a supercritical fluid, respectively.

c) *Determine Reynolds numbers for these parameters, assuming a grain size of 0.1 mm and fluid density values from question 5.*

Using Equation 1.65, we obtain a local Reynolds number of $R_e = 1.8 \times 10^8$ for brine and $R_e = 9.4 \times 10^1 0$ for supercritical fluid, respectively.

d) *Do these values of Reynolds number meet the assumptions for Darcy's Law?*

Darcy's Law assumes $R_e \ll 1$. Clearly, tthese values of Reynolds number do not meet the assumptions for Darcy's Law.

## 1.7 Online Exercise

Recent studies have highlighted the potential significance of pore-fluid pressure as a factor that may control the onset, termination and distribution of seismicity induced by fluid injection into the subsurface. In a porous medium, the diffusion of pore-fluid pressure is described by Equation 1.56.

The Coulomb Failure Function (CFF) is a commonly used criterion to characterize failure on pre-existing or incipient fault planes (King et al., 1994; Lin and Stein, 2004; Toda et al., 2005). For a given fault orientation defined by a surface normal $\hat{\mathbf{n}}$, CFF is defined as

$$CFF = |\tau(\mathbf{n})| - \mu_{\mathbf{f}}(\sigma_{\mathbf{n}}(\mathbf{n}) - \mathbf{P}),$$

where $\tau(\hat{\mathbf{n}})$ is the shear stress acting on the plane, $\mu_f$ is the effective coefficient of friction, $\sigma(\hat{\mathbf{n}})$ is the normal stress on the fault and $P$ is the pore-fluid pressure. If stress conditions are changed, $\Delta CFF$ is considered as a fault failure index; hence, if $\Delta CFF > 0$, it indicates that the fault plane has moved closer to failure, whereas if $\Delta CFF < 0$, it indicates that a fault plane has moved farther from failure.

During hydraulic fracturing, one of the ways in which CFF can change is due to a change to pore pressure. Recent studies have highlighted the potential significance of pore-fluid pressure as a factor that may control the onset, termination and distribution of seismicity induced by fluid injection into the subsurface. Here, a simple Matlab tool is provided to visualize pore-pressure diffusion and to investigate parameter sensitive, including:

- Permeability of the background medium.
- Viscosity of the injected fluid.
- Injection duration.
- Fracture orientation.
- Injection pressure.

### 1.7.1 Procedure

Open the file **frac_mod** in a Matlab window. When you run this, you are prompted to enter input values using a series of dialog boxes, as shown below.


The default parameters shown above are based on Langenbruch and Shapiro (2010). The viscosity is for slickwater at a depth of 2 km.

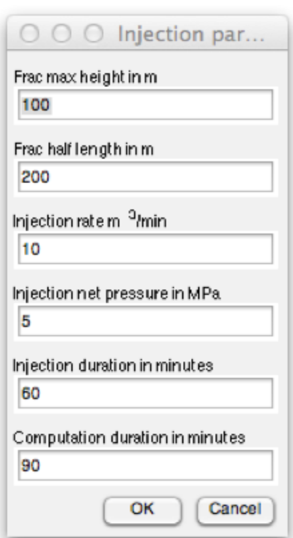

These parameters are meant to be representative of a typical treatment stage. The frac height cannot be too much larger without interference with the edge of the computational grid, which is 500m high and 2000m wide. Here **n** denotes the normal to pre-existing fractures, which in this case are vertical since the $z$-component is set to zero.

The first step in program execution is to calculate pore-pressure diffusion for the case of an expanding tensile fracture in a homogeneous, isotropic poroelastic medium.

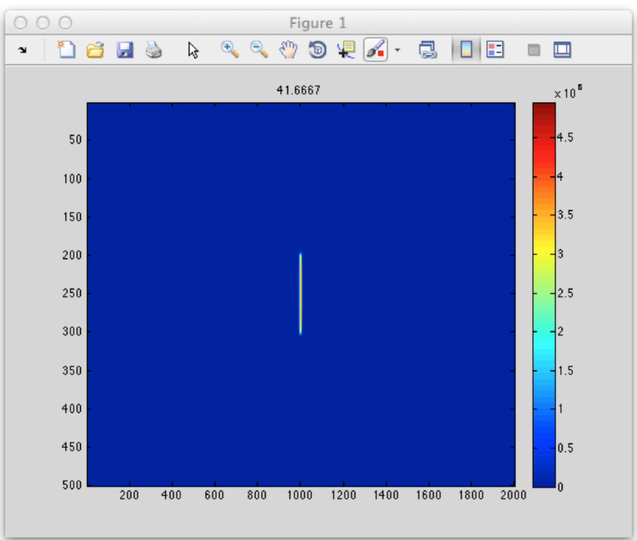


This is a purely illustrative snapshot of the pore pressure (in units of Pa) at 41.67 minutes after initiation of injection. The fracture has grown to its full height of 100m. The $x$- and $y$-units are metres.

Once the program has finished execution, three plots are generated showing the CFF change due to a) pore pressure changes alone; b) stress change alone; c) both pore pressure and stress change. Examples of these plots are given below.

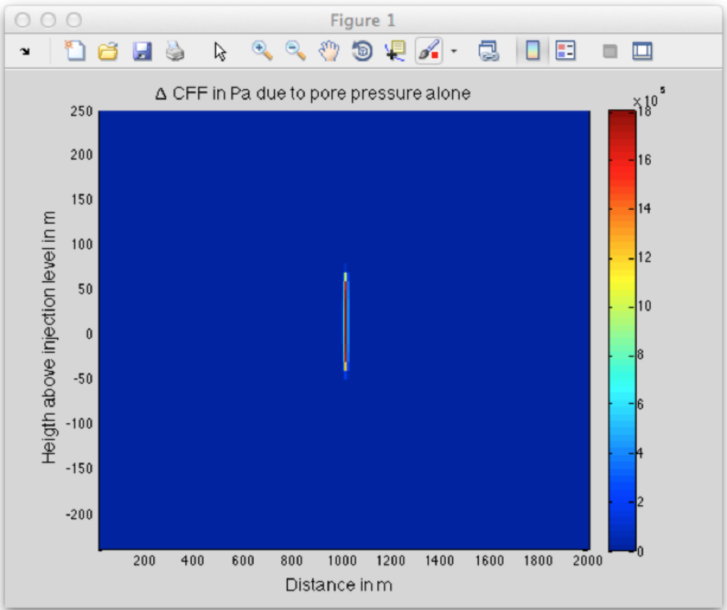
Figure 1
Δ CFF in Pa due to pore pressure alone
Heigth above injection level in m
Distance in m
x 10^5

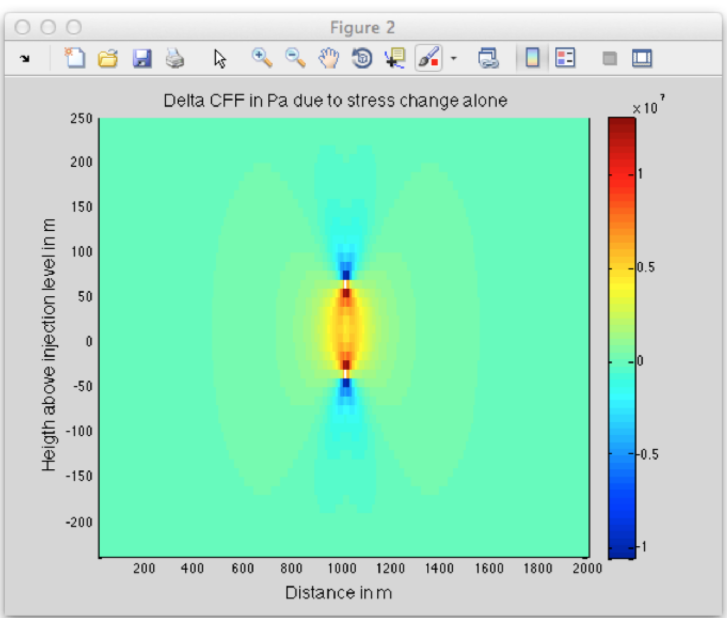
Figure 2
Delta CFF in Pa due to stress change alone
Heigth above injection level in m
Distance in m
x 10^7

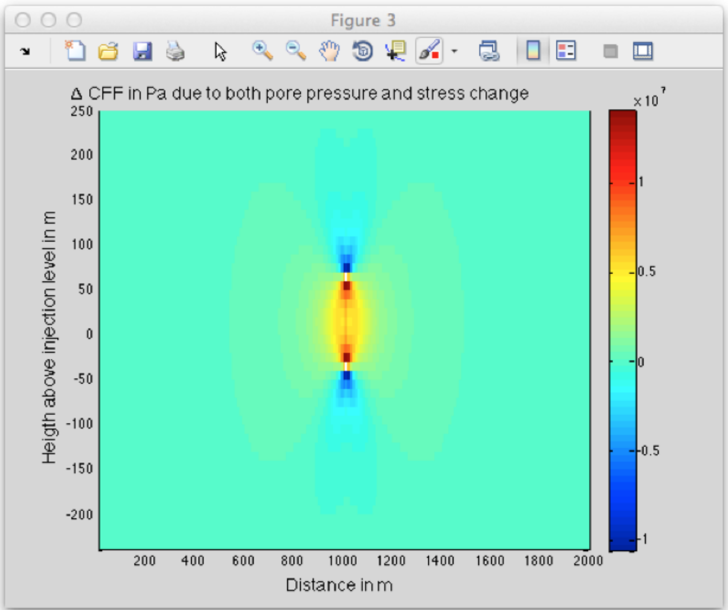


Try experimenting with parameters, including:

- Permeability of the background medium and viscosity of the fluid; in a more permeable medium, the pore pressure will diffuse farther within the time-frame of the frac treatment.
- Duration of the treatment. Try capturing the results right at the end of the treatment, rather than 30 minutes later as in the default settings.
- Normal directions for pre-existing fractures.
- Net injection pressure.

Be forewarned that some choices of parameters will render the execution of the program numerically unstable. Also, note that the growth of the hydraulic fracture depicted in these examples is imposed here based on an assumed growth rate and does not reflect a numerical simulation of physical fracture growth.

# 2 Chapter 2

## 2.1 Problem 1

*Consider a tensile (mode-I) crack as depicted in Figure 2.3.*

a) *Given $K_I/\sqrt{2\pi r}$ = 1.0 MPa, calculate the 2D stress tensor at $\theta$ = 0°, 30° and 90° from the tip of a mode-I fracture (using Equations 2.3 - 2.5)*

Using Equations 2.3 - 2.5, the corresponding 2D stress tensors are:

For $\theta = 0$, $\boldsymbol{\sigma} = \begin{bmatrix} 1.0 & 0 \\ 0 & 1.0 \end{bmatrix}$ MPa

For $\theta = 30°$, $\boldsymbol{\sigma} = \begin{bmatrix} 0.79 & 0.18 \\ 0.18 & 1.14 \end{bmatrix}$ MPa

For $\theta = 90\circ$, $\boldsymbol{\sigma} = \begin{bmatrix} 0.35 & -0.35 \\ -0.35 & 1.06 \end{bmatrix}$ MPa

b) *Assuming $K_I/\sqrt{2\pi r}$ = 1.0 MPa, what is the normal stress for each of the values of $\theta$, for a planar surface that is oriented 30° from the fracture plane? What is the shear stress?*

The normal and shear stress can be determined from the traction $\mathbf{T} = \hat{\mathbf{n}} \cdot \boldsymbol{\sigma}$, where the normal to the surface is $\hat{\mathbf{n}} = (-\sin 30°, \cos 30°)$. The normal stress acting on this surface is:

$\sigma_n = \mathbf{T} \cdot \hat{\mathbf{n}}' = 0.90$ MPa.

The magnitude of the shear stress is given by $(|\mathbf{T}|^2 - \sigma_n^2)^{1/2} = 0.24$ MPa.

c) *Repeat the above calculations for a surface that is parallel to the main model-I fracture.*

In this case, the normal stress is $\sigma_n = 1.0$ MPa and the shear stress is zero.

d) *Which regions in the vicinity of the fracture tip are in tension? Which regions have elevated shear stress?*

The region directly in front of the fracture tip is in tension, whereas the region oblique to the fracture tip (e.g. point $P$ in Figure 2.3) has elevated shear stress.

## 2.2 Problem 2

*A set of laboratory measurements on a sample of dolomite indicates that the unconfined (or uniaxial) compressive strength ($\mathcal{S}$) is 250 MPa.*

a) *Determine the cohesion, for $\mu_i$ = 1.0.*

Using Equation 2.9, the cohesion is given by $\mathcal{C} = 51.8$ MPa.

b) *Assuming $\sigma_3$ = 15 MPa, determine $\sigma_1$ at the point of failure, based on the Mohr-Coulomb criterion.*

The maximum principal stress at the point of failure is given by

$$\sigma_1 = \left[(\mu_i^2+1)^{1/2}+\mu_i\right]^2 \sigma_3 + 2\mathcal{C}\left[(\mu_i^2+1)^{1/2}+\mu_i\right] = 337.4 \text{ MPa} .$$

c) *Calculate $\sigma_1$ at the point of failure based on the Hoek-Brown criterion for an intact rock, using the mean value of the material constant $m$ for dolomite given in Table 2.1.*

Using $m = 6.5$ and $s = 1$ (for intact rock), Equation 2.11 gives $\sigma_1 = 309.7$ MPa.

d) *Calculate $\sigma_1$ at the point of failure using the modified Lade criterion, assuming that $\sigma_2$ is the mean of the maximum and minimum principal stresses.*

Recalling that $\phi_i = \tan^{-1}(\mu_i)$, $\sigma_1$ can be determined numerically through an iterative process, by evaluating Equations 2.13 - 2.15 until Equation 2.12 is satisfied. An approximate solution obtained using this approach is $\sigma_1 = 622.4$ MPa. Clearly, the Lade criterion predicts considerably greater rock strength than the previous methods.

## 2.3 Problem 3

*Consider a point in the subsurface at a depth of 3000 m. Assuming a linear density gradient given by $\rho(z) = 2200 + 0.14z$, where $\rho$ is in kg/m$^3$ and $z$ is in m, calculate the following.*

a) *Determine $S_V$.*

The vertical stress at depth $z$ is given by $S_V = g\int_0^z \rho(z)dz$. For a linear density gradient $\rho(z) = \rho_0 + kz$, we have $S_V = \int_0^z(\rho_0 + kz)dz = g(\rho_0 z + \frac{kz^2}{2})$. Based on the parameters given above and $g = 9.8$ m/s$^2$, $S_V = 70.9$ MPa.

b) *If the pore-pressure gradient is 15 kPa/m and the Biot coefficient ($\alpha$) is 0.5, determine $S'_V$.*

The pore pressure at depth $z$ is $P(z) = k_P z$, where $k_P$ is the pore-pressure gradient. At $z = 3000$m, the pore pressure is 45 MPa for $k_P = 15$ kPa/m. For a Biot coefficient of $\alpha = 0.5$, the effective vertical stress is $S'_V = S_V - \alpha P = 48.4$ MPa.

c) *For a critically stressed state in an extensional faulting regime with $\mu_s = 0.6$, what is $S'_{Hmin}$?*

Using Equation 2.17, $S'_{Hmin} = S_{Hmin} - \alpha P = 15.5$ MPa.

d) *For a critically stressed state in a strike-slip faulting regime with $\mu_s = 0.6$, what is $S'_{Hmin}$ assuming that $S'_V$ is the average of $S'_{Hmax}$ and $S'_{Hmin}$?*

In this scenario, $S'_V = \dfrac{S'_{Hmax} + S'_{Hmin}}{2}$. Therefore $S'_{Hmax} = 2S'_V - S'_{Hmin}$. Substituting this into Equation 2.18 and solving gives $S'_{Hmin} = 23.5$ MPa.

## 2.4 Problem 5

*Assuming that a slip surface is in a critically stressed state before and after rupture as shown in Figure 2.15, calculate the stress drop if $\sigma_1 = 40$ MPa, $\sigma_3 = 15$ MPa, $\mu_s = 0.6$, $mu_r = 0.4$ and $\mathcal{C} = 5$ MPa.*

In the initial, critically stressed state, the angle $\theta$ between the fault normal and the maximum principal stress axis is given by (see Figure 1.2):

$$\theta = \frac{\frac{\pi}{2} + \tan^{-1}\mu_s}{2}.$$

For a co-ordinate system in which the axes are aligned with the principal stress directions, the fault normal vector is $\hat{\mathbf{n}} = (\cos\theta, 0, \sin\theta)$. Given $\sigma_1$ and $\sigma_3$ above, the normal stress acting on this plane is 33.9 MPa. From Equation 2.24, the stress drop is therefore $\Delta\tau = 11.8$ MPa.

## 2.5 Problem 6

*Suppose that the Voigt model depicted in Figure 2.16a is subject to an abrupt increase in applied stress, $\sigma$. As outlined by Courtney (2000), the parallel configuration of the spring and dashpot in this model means that strain is equal for both elements, but the stress is partitioned such that the total stress is $\sigma = \sigma_{sp} + \sigma_d$, where the subscripts sp and d denote the spring and dashpot, respectively. At the instant the stress is applied, the stress is carried entirely by the dashpot; over time, the stress is gradually transferred to the spring. Find analytical expressions for the temporal behaviour of $\sigma_{sp}, \sigma_d, \epsilon$ and $\dot{\epsilon}$.*

Let $t = 0$ denote the time at which the stress is applied. The constitutive (stress-strain) behaviour of the two elements of the Voigt solid are $\sigma_{sp} = E\epsilon$ for the spring, and $\sigma_d = \eta\dot{\epsilon}$ for the dashpot. Since the applied stress is constant for $t > 0$ and is represented by the sum of the stress in each of the elements, the time derivative of the stress is

$$E\dot{\epsilon} + \eta\ddot{\epsilon} = 0.$$

Integrating this expression over time leads to

$$\dot{\epsilon} = \dot{\epsilon}_0 e^{-\frac{E}{\eta}t},$$

where $\dot{\epsilon}_0$ denotes the strain rate at $t = 0$. At the instant the stress is applied, all of the stress is carried by the dashpot; hence

$$\dot{\epsilon}_0 = \frac{\sigma}{\eta}.$$

Given the constitutive relationships for the dashpot, we then have

$$\sigma_d = \sigma e^{-\frac{E}{\eta}t}.$$

To obtain the stress in the spring, we need to integrate a second time using the initial strain rate. This leads to

$$\epsilon = \frac{\sigma}{E}\left(1 - e^{-\frac{E}{\eta}t}\right).$$

Hence the stress in the spring is $\sigma_{sp} = \sigma(1 - e^{-\frac{E}{\eta}t})$. The stress is therefore initially carried entirely by the dashpot, but over time it shifts to the spring. Thus, as the $t \to \infty$, the strain approaches $\frac{\sigma}{E}$.

## 2.6 Online Exercise

Mohr diagrams are useful for visualizing the state of stress in addition to various forms of failure criteria. A Matlab tool is provided to depict 3D Mohr diagrams under varying stress conditions, including the stress acting on fractures with random orientation.

### 2.6.1 Procedure

1 Open Matlab and ensure that your path is properly configured, as described in the getting started documentation. From the Matlab prompt, type open Mohr_tool. A new window will open showing the Matlab code.
2 Run the script using default values. To run the script, press the green arrow at the top of the screen.
3 Make the intact rock fail in shear slip, by adjusting the fracture parameters (cohesion and fraction) so that they are the same as the intact medium, and adjusting the stress parameters and pore pressure as needed to cause failure.
4 Induce tensile failure in the intact rock, using the same process as described above.
5 Experiment with a stress state that has low differential stress, $\sigma_2 \simeq \sigma_3$.

# 3 Chapter 3

## 3.1 Problem 1

*Find a rotation operator that transforms the diagonal form of the double-couple moment tensor in Equation 3.62 into a tensor form with two shear couples.*

An operator that applies a clockwise rotation about the $x_2$ axis of $\theta = -45°$ (see Box 1.1), or equivalently a counter-clockwise rotation of 45°, will transform the moment tensor in Equation 3.62 into a tensor form with two shear couples. The rotation matrix has the form:

$$\mathbf{R} = \begin{bmatrix} \cos\theta & 0 & \sin\theta \\ 0 & 1 & 0 \\ -\sin\theta & 0 & \cos\theta \end{bmatrix}.$$

The transformed moment tensor is given by

$$\mathbf{M} = \begin{bmatrix} 0 & 0 & 1 \\ 0 & 0 & 0 \\ 1 & 0 & 0 \end{bmatrix}.$$

## 3.2 Problem 2

*Within Anderson's classification scheme, what type of event is represented by the double-couple (DC) solution in Figure 3.15?*

The DC solution in Figure 3.15 can be described as an approximately strike-slip event, with a component of reverse motion. This hybrid mechanism is sometimes called oblique slip.

## 3.3 Problem 3

*By solving Equation 3.25, determine the fundamental-mode Love-wave velocity at frequencies of 10 Hz and 20 Hz, for a simple model with a 12 m thick layer with $v_S$ = 250 m/s and $\rho$ = 1800 kg/m$^3$ overlying a half space with $v_S$ = 1250 m/s and $\rho$ = 2250 kg/m$^3$.*

By numerical solution of Equation 3.25 (see Figure 3.2) the fundamental-mode Love-wave velocity is found to be 291.3 m/s at 10 Hz and 258.8 m/s at 20 Hz.

## 3.4 Problem 4

*Suppose that phase velocity within the frequency band $0 < f < \pi$ is given by $v = v_1 + A\cos(f/B)$. Use Equation 3.26 to find an expression for the group velocity within this band.*

By applying the chain rule, Equation 3.26 can be rewritten as

$v_g = v + \omega \frac{\partial v}{\partial \omega}$.

Substituting the above expression for phase velocity leads to

$v_g = v_1 + A\cos(f/B) - \frac{A\omega}{2\pi B}\sin(f/B)$.

## 3.5 Problem 5

*Consider a planar interface between two isotropic elastic half spaces characterized by $v_{P1}$ = 2100 m/s, $v_{S1}$ = 1000 m/s and $\rho_1$ = 2200 kg/m$^3$ in the upper half space, with $v_{P2}$ = 4600 m/s, $v_{S2}$ = 2600 m/s and $\rho_2$ = 2200 kg/m$^3$ in the lower half space. Determine all of the critical angles for incident plane waves ($P$, $S_V$ and $S_H$) in the upper medium. Discuss how the post-critical reflections might impact wide-angle recordings using a downhole microseismic array.*

For an incident $P$ wave, there are two critical angles corresponding to the refracted $P$ and $S_V$ waves in the lower medium; using Snell's Law, these angles are 27.2° and 53.9°, respectively. For an incident $S_V$ wave, there are also two critical angles corresponding to the refracted $P$ and $S_V$ waves in the lower medium; these angles are 12.6° and 22.6°, respectively. In the case of an incident $S_H$ wave, there is only one critical angle that corresponds with the refracted $S_H$ wave in the lower medium. The critical angle is 22.6°.

For downhole microseismic monitoring the raypaths are usually close to horizontal, leading to common grazing incidence at horizontal boundaries. This geometry will produce an abundance of post-critical reflections for the scenario considered here.

## 3.6 Problem 6

Using $Q_P = 100$, 500, $Q_S = 50$, 250, plot Brune and a Boatwright spectra at $t = 5$ s for all $Q$ values, for a source with a corner frequency of $f = 5.0$ Hz.

The following graphs were computed in Matlab for the set of $Q$ values specified above. The top row shows $S$-wave spectra, while the bottom row shows $P$-wave spectra. As expected, the Boatwright spectra are characterized by a sharper corner.

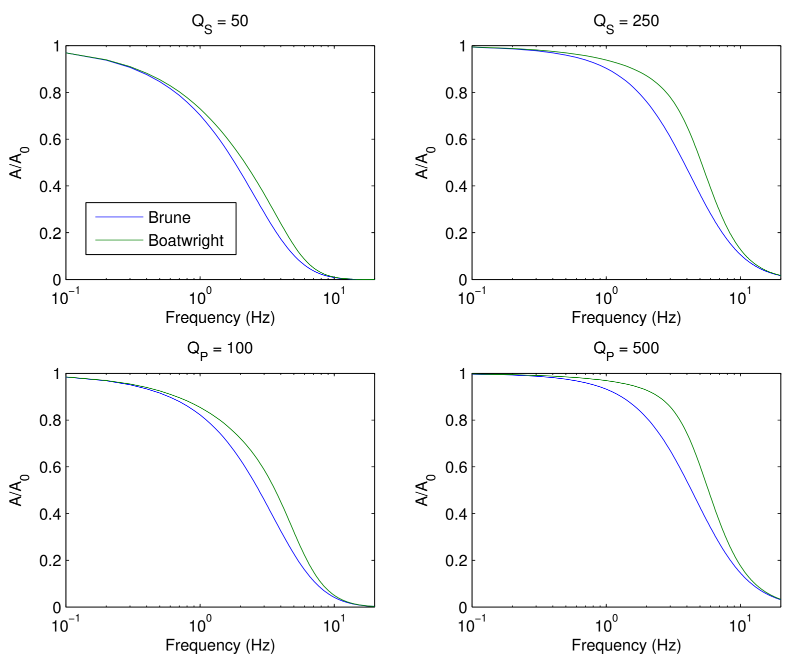


## 3.7 Problem 7

*Consider a fault with strike of 30°, dip of 70° and rake of 10°.*

a) *Calculate the vectors corresponding to the* $\hat{\mathbf{d}}$, $\hat{\mathbf{n}}$, $\hat{\mathbf{t}}$, $\hat{\mathbf{b}}$, *and* $\hat{\mathbf{p}}$ *axes.*

Using Equations 3.69 - 3.71, these unit vectors have the following values:

$\hat{\mathbf{d}}$ = (0.88,0.44,-0.16)
$\hat{\mathbf{n}}$ = (-0.47,0.81,-0.34)
$\hat{\mathbf{t}}$ = (0.29,0.89,-0.36)
$\hat{\mathbf{b}}$ = (0.02,-0.38,-0.93)
$\hat{\mathbf{p}}$ = (-0.96,0.26,-0.13)

f) *Write the moment tensor using geographic coordinates*

Using Equation 3.67, the moment tensor can be written in geographic coordinates as

$$\mathbf{M} = \mu A \begin{bmatrix} -0.83 & 0.51 & -0.23 \\ & 0.72 & -0.28 \\ & & 0.11 \end{bmatrix}.$$

g) *Write the moment tensor in diagonalized form.*

The diagonalized moment tensor has the same form as Equation 3.62, multiplied by the factor $\mu A$.

## 3.8 Problem 8

*The surface projection of the rupture zone for a 30°-dipping reverse fault is 3 km long and 0.25 km in width. The slip function on the fault can be approximated a three fault segments that occupy 50%, 30% and 20% of the fault surface area, with uniform slip of 40 cm, 30 cm and 20 cm (respectively) within each of these ruptures zones. Assuming that the shear modulus is $\mu$ = 10 GPa, what is the seismic moment? What is the corresponding moment magnitude?*

Based on the information given above, the fault area is:

$A = 3000 \times 250/\cos 30° = 8.66 \times 10^5$ m$^2$.

The average slip $\bar{d}$ is an area-weighted average of the slip in each of the rupture zones, 0.33 m. The seismic moment is given by Equation 3.66 and is the product of the average slip, rupture area and shear modulus, 2.86 $\times 10^{15}$ N-m. The moment magnitude can be determined from Equation 3.81 and is 4.3.

## 3.9 Problem 9

*After a large earthquake, the number of recorded aftershocks per day after 1, 4 and 20 days is 80, 18 and 3 per day. Using Equation 3.98 (generalized Omori's law), estimate the parameters $k$, $c$ and $p$.*

Through a process of trial and error, the aftershock rate, $r_a(t)$, can be approximated using parameters $k = 105$, $c = 0.26$ days and $p = 1.2$, where $t$ is in days.

## 3.10 Online Exercises

a) The Zoeppritz equations can be solved numerically to visualize the amplitude and phase of reflected and transmitted plane waves at a planar interface between two elastic half spaces that are in welded contact. A Matlab tool is provided that facilitates graphical exploration of $P - S_V$ energy partitioning at an interface.

b) Source-type diagrams developed by Hudson et al. (1989) provide a convenient way to classify the type of rupture (double couple, tensile crack opening, compensated linear vector dipole, etc.), irrespective of geometry of the source. A visualization tool is provided to project an arbitrary moment tensor into this diamond-shaped graph.

### 3.10.1 Procedure

Open Matlab and ensure that your path is properly configured, as described in the getting started documentation. From the Matlab prompt, type zprtz_tool. This will open a dialog box as illustrated below.

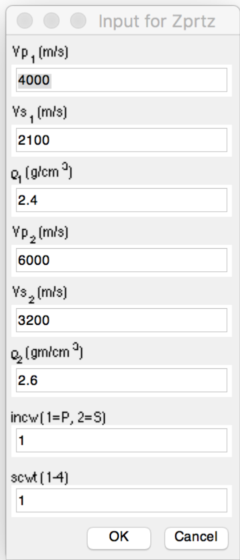


Apart from the last two, most of the input parameters are self-explanatory. The incident wave type (medium 1) is denoted as incw and takes the values 1 for an incident $P$ wave and 2 for an incident $S$ waves. The scattered wave type is denoted as scwt and takes the following values:

1. Reflected $P$ wave

2. Reflected $S_V$ wave

3. Transmitted $P$ wave

4. Transmitted $S_V$ wave

The graph generated by the program using default parameters is shown below. The top panel shows the amplitude of the reflection/transmission coefficient, while the lower panel shows the phase. In this case, the critical angle angle for the $P-P$ reflection is about $42°$. Try experimenting with different values for the input parameters.

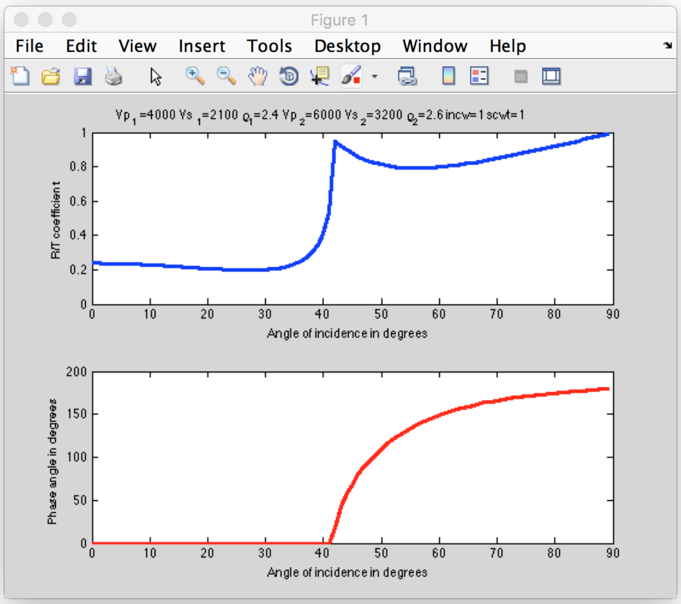


Next, type **stp_tool** to bring up the following dialog box for the source-type plotting program:

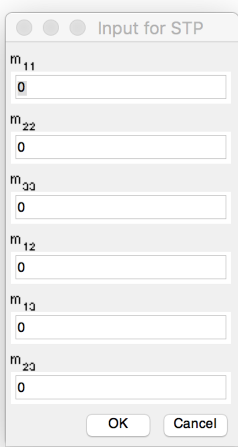


Input parameters are the components of a moment tensor. The program prompts to enter additional moment tensors, each of which is projected into a Hudson plot as illustrated below.

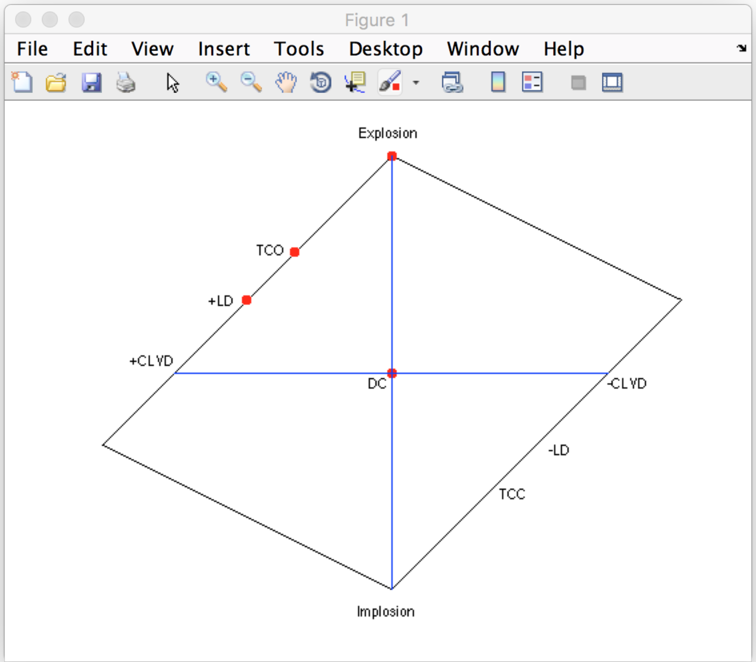
Figure 1
File Edit View Insert Tools Desktop Window Help
Explosion
TCO
+LD
+CLVD
DC
-CLVD
-LD
TCC
Implosion

# 4 Chapter 4

## 4.1 Problem 1

*$S_{Hmin}$ = 44.0 MPa has been estimated based on observation of the fracture closure pressure (FCP) from an extended leakoff test (XLOT).*

a) *Use Equation 4.6 to estimate $S_{Hmax}$, neglecting the generated hoop stress $\Delta\sigma_{\theta\theta}$ and assuming $\Delta\Theta$ (angular breakout width) = 20° and $\mathcal{S}$ (unconfined compressive strength) = 150 MPa.*

Using Equation 4.6 and the parameters given above, $S_{Hmax} = 65.6$ MPa.

b) *If $P_R$ = 49 MPa, use this estimate for $S_{Hmax}$ to estimate the pore pressure, $P$.*

Equation 4.9 gives $P = 17.5$ MPa.

c) *Why is it not possible to infer $S_{Hmax}$ in a reverse faulting environment?*

The XLOT test provides an estimate of the minimum principal stress. In a reverse faulting environment, the minimum principal stress is vertical; hence, it is not possible to infer the minimum horizontal stress.

## 4.2 Problem 2

*Using the same model for density and pore-pressure gradient as in question 3 from chapter 2, and assuming the generalized strain model, calculate the effective principal stresses $S'_V, S'_{Hmax}$ and $S'_{Hmin}$ given a Biot parameter of $\alpha$ = 0.5, tectonic strains of $\epsilon_H = 10^{-3}$ and $\epsilon_h = 10^{-4}$, and a shear modulus of $\mu$ = 10 GPa. Assume a Poisson solid ($\nu$ = 0.25). This approach is sometimes called a mechanical Earth model.*

As outlined in the solution for problem 3 in chapter 2, we have $S_V = 70.9$ MPa at 3.0 km depth. For a pore-pressure gradient of 15 kPa/m, this leads to an effective vertical stress of $S'_V = 48.4$ MPa. The generalized strain model is represented by

Equations 4.19 - 4.20. Based on these expressions, $S'_{Hmax}$ = 43.5 MPa and $S'_{Hmin}$ = 25.5 MPa.

## 4.3 Problem 3

*Consider a hydraulic fracture of fixed height $h_f$ = 30 m. Assuming a Perkins-Kern-Nordgren (PKN) model, calculate the following at time t = 30 minutes, given a constant injection rate of $q_i$ = 8 $m^3$/min, dynamic viscosity $\eta$ = $10^{-3}$ Pa-s and an average fracture width (or aperture) of 2 mm. Assume that the medium is characterized by a Young's modulus of E = 20.0 GPa, a Poisson's ratio of $\nu$ = 0.3 and a leakoff coefficient given by $C_L$ = 0.002 m $min^{-1/2}$.*

a) *The fracture area as a function of time, $A_f(t)$.*

Using Equation 4.27, at $t = 30$ minutes $A_f(t) = 7.28 \times 10^3$ m$^3$.

b) *The fracture length, for a simple case of a fracture with a rectangular cross section.*

For a vertical fracture of rectangular shape, the length is the area divided by the height or 242.5 m.

c) *The net pressure, $P_{net}$.*

Based on Equation 4.23, $P_{net}$ = 1.2 MPa. Be mindful of units and note that the plane-strain modulus ($E'$) must be calculated.

d) *The fracture width (also known as fracture aperture) at the $x = 0.5L$, using Equation 4.24. Compare this with the assumed average width given above.*

The calculated value for the fracture aperture is 0.0028 m. This is somewhat greater than the average width of 2.0 mm given above, but is reasonable considering that the fracture aperture is reduced near the tip.

## 4.4 Problem 4

*Use the Khristianovich-Geertsma-de Klerk (KGD) model with the parameters given in the previous question to compute the following.*

a) *The fracture length (L).*

Using Equation 4.29, the approximate fracture length is given by $L \approx 116.2$ m.

b) *The net pressure.*

Using Equation 4.28, $P_{net} = 5.3$ MPa.

## 4.5 Problem 5

*Calculate the terminal proppant settling velocity based on Stoke's Law (Equation 4.31) using the dynamic viscosity given in question 3. Assume the maximum grain diameter at 90% probability for a 20/40 mesh, and a density contrast of 1500 kg/m$^3$ between the proppant grains and the fluid.*

From Table 4.1, the maximum grain diameter at 90% probability for a 20/40 mesh is 850 $\mu$m. Given the other parameters listed above, the terminal proppant settling velocity is 0.59 m/s.

## 4.6 Problem 6

*The hydraulic injected energy is given by $E = \int_{t_1}^{t_2} PR\, dt$, where $P$ is the injection pressure and $R$ is the injection rate. For a constant bottomhole injection pressure of $P = 50$ MPa and a uniform injection rate of $R = 8$ m$^3$/min, calculate the total hydraulic injected energy from $t_1 = 0$ to $t_2 = 30$ minutes. Use Equation 3.87 to calculate the magnitude of an earthquake with the equivalent radiated seismic energy.*

Since the pressure and rate are assumed constant, the above integral reduces to a simple product, yielding $E = 1.2 \times 10^{10}$ J. From Equation 3.87, the equivalent earthquake has a moment magnitude of 3.52.

# 5 Chapter 5

## 5.1 Problem 1

*Use Equations 5.1-5.3 to estimate the minimum magnitude for a locatable event, at a distance of $r$ = 500 m and a frequency of $f_0$ = 15 Hz. Start by calculating the seismic moment, assuming that the amplitude with 10% probability of detection ($A_{10}$) is 0.1 $\mu$m; then calculate the corresponding moment magnitude using Equation 5.3. Use the following parameters: $v_P$ = 4000 m/s, $v_S$ = 2000 m/s, $\rho$ = 2500 kg/m$^3$, $Q_P$ = 200 and $Q_S$ = 100.*

From Equation 5.1, $M_0^P = 5.0 \times 10^7$ N-m and from Equation 5.2, $M_0^S = 1.1 \times 10^7$ N-m. In order to locate an event, both the $P$ and $S$ wave must be above the detection limit. We therefore use the $P$ wave to determine the magnitude, yielding $M_W$ = -0.9.

## 5.2 Problem 2

*Design a linear geophone array using Equation 5.4, for which the first notch rejects horizontally propagating waves such as ground roll with a frequency $f$ = 10 Hz and an apparent horizontal velocity of 500 m/s.*

The reader may notice that the number of elements in the linear array is not specified; this is because it is the effective array length ($L = n\Delta x$) that is important in this calculation. As shown in Figure 5.8, the first notch coincides with $\lambda_A = L$. For the parameters given above, $\lambda_A$ = 50 m.

## 5.3 Problem 3

*Suppose that the mass element of a 10 Hz geophone is 100 g.*

a) *What is the spring constant, $k$?*

From Equation 5.6 we see that

$$k = 2\pi f_0^2 M = 62.8 \text{ kg s}^{-2} .$$

b) *Assuming that the geophone is critically damped and has a sensitivity of $S_g = 1$, what is the amplitude and phase of the transfer function at 2 Hz and 20 Hz?*

The geophone transfer function expressed by Equation 5.7 gives a Complex result, which can be represented in terms of amplitude and phase. For a critically damped geophone, the damping factor is $\lambda_g = \frac{1}{\sqrt{2}}$. For $f = 2$ Hz, which falls significantly below the natural frequency of the geophone, the amplitude of the transfer function is 0.04 and the phase is -16.4°. For $f = 20$ Hz, above the natural frequency of the geophone, the amplitude of the transfer function is 0.97 while the phase is -136.7°. In the limit as $f \to \infty$, the geophone transfer function approaches an amplitude of unity and a phase of -180°.

## 5.4 Problem 4

*A seismometer has a sensitivity of 1000 V/m/s, 2 poles at +/- 4.4 Hz and 2 zeros at 0 Hz. Calculate the amplitude and phase of the instrument response at 2 Hz and 20 Hz.*

The seismometer transfer function is given in Equation 5.9. For the parameters specified above, the transfer function works out to be 890.8 V/m/s at $f = 2$ Hz and 998.8 V/m/s at $f = 20$ Hz. In both cases, the phase response is zero.

## 5.5 Problem 5

*Consider a four-station surface network, at locations that are 3.0 km to the north, south, east and west of an event with hypocentre at 4000 m depth. Assume that the medium is homogeneous and isotropic with velocity $V$.*

a) *Calculate the Fréchet derivative matrix of traveltimes, $A_{ij} = \frac{\partial t_i}{\partial x_j}$. Here, $i$ denotes* *the station number and* $j$ = *1,2,3 denotes* $x, y$ *and* $z$ *location indices for the source.*

Let the four stations be arranged so the $i = 1, 2, 3, 4$ corresponds to stations located north, south, east and west of the event and consider the 2-D problem with $j = 1, 2$ representing east and north spatial coordinates, respectively. If the hypocentral distance is denoted by $r$, then from the chain rule the derivative computed in the direction of the station offset is

$$\frac{\partial t}{\partial x} = \frac{\partial t}{\partial r}\frac{\partial r}{\partial x} = \frac{1}{V}\frac{x}{r} = p,$$

where $p$ is the horizontal slowness in the direction of the station. The Fréchet derivative matrix is therefore given by

$$\mathbf{A} = \begin{bmatrix} 0 & p \\ 0 & -p \\ p & 0 \\ -p & 0 \end{bmatrix}.$$

b) *Calculate* $\det(\mathbf{A^T A})$*, which is the basis for the D-optimality criterion for survey design.*

The matrix $\mathbf{A^T A}$ can be written as:

$$p^2 \begin{bmatrix} 2 & 0 \\ 0 & 2 \end{bmatrix}.$$

Evaluating the determinant of this matrix, $\det(\mathbf{A^T A}) = 4p^2$.

## 5.6 Online Exercises

.

A set of Matlab tools is provided to aid in visualization of uncertainty for parameters associated with the design of a passive-seismic experiment. These tools can be used to create graphs of seismic-detection probability versus distance, as a function of injected fluid volume, stochastic diagrams of location uncertainty and condition number for moment-tensor inversion.

### 5.6.1 Procedure

1. Use the Matlab program MSD_detect to generate examples of seismic detection probability as a function of injected fluid volume. Try adjusting the input parameters (seismic efficiency, noise level, distance range, etc.) to get a feel for inherent tradeoffs. Note: the background noise factor is a scalar for the USGS NHNM at 10 Hz. A sample screen shot is shown below.

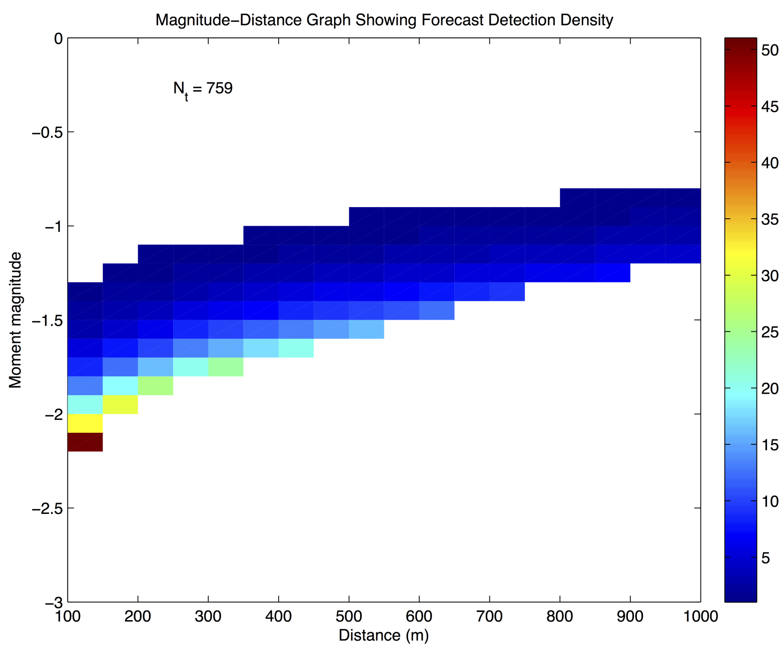


2. Use the Matlab program MSD_locerr to generate stochastic diagrams of location uncertainty. This program uses a homogeneous velocity model to compute synthetic locations based on $P$ and $S$ arrival times plus $P$-wave inclination and azimuth. Random errors (zero mean, uniform deviates) for 50 realizations are added to the pick times and polarization data. A sample screen shot of the 3D perspective view generated by the program is shown below. Receivers are shown by green triangles, true source locations with magenta circles, and stochastic source points with black + symbols.

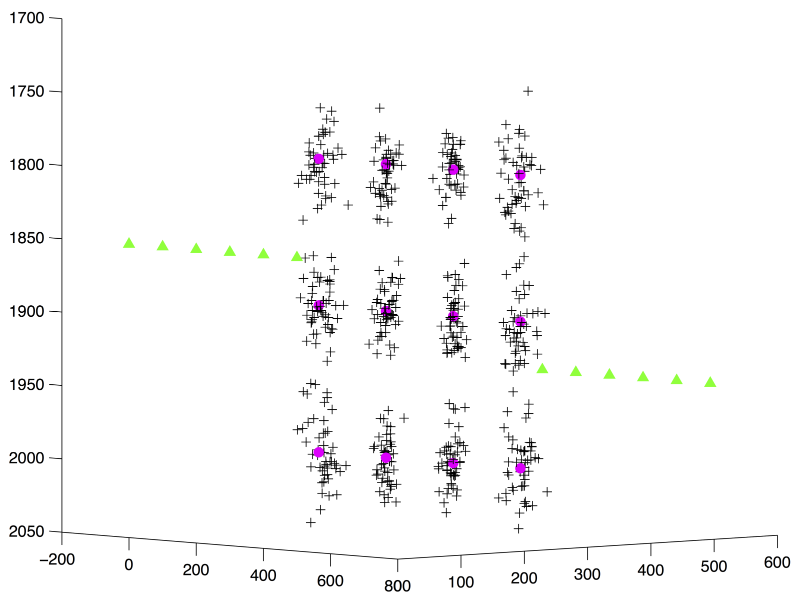


The following scenarios are defined by receiver location files:

- sensors.txt: single vertical monitor well located above the reservoir horizon
- sensors2.txt: a deviated monitor well that spans the reservoir horizon
- sensors3.txt: a single horizontal receiver array within the reservoir horizon
- sensors4.txt: two horizontal monitor wells on both sides, slightly offset in depth
- sensors5.txt: three sparse vertical monitor arrays around the reservoir
- sensors6.txt: two sparse vertical monitor wells on one side
- sensors7.txt: a surface cross-arm array

3. Use the Matlab program MSD_mti to compute the moment tensor inversion (MTI) condition number for all of the above sensor geometries. A sample screen shot is shown below. This is a map view. Receivers are indicated by black triangles. In general, the condition number should be as small as possible for stable inversion results.

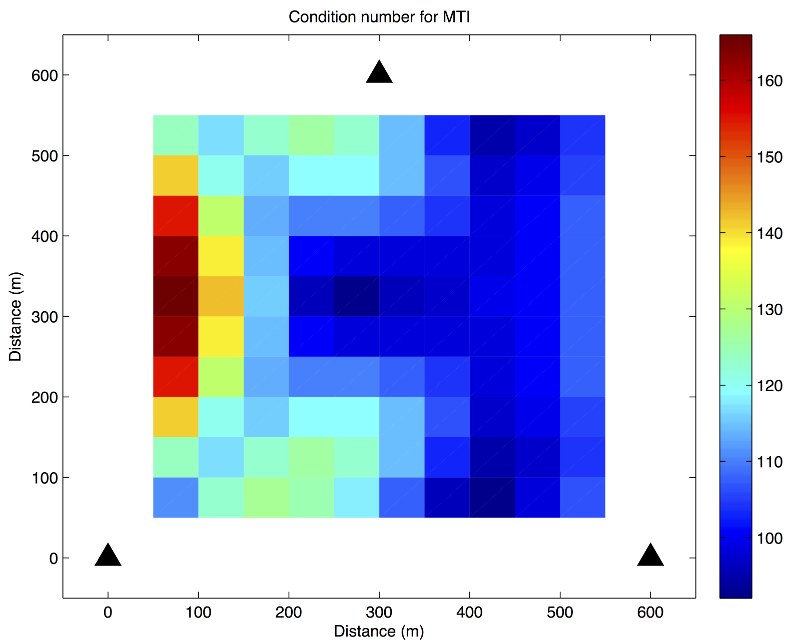
Condition number for MTI
Distance (m)
Distance (m)
0
100
200
300
400
500
600
100
110
120
130
140
150
160

# Chapter 6

## 6.1 Problem 1

*Suppose that recorded ground motion as a function of time $t$ ($0 < t < T = N\pi$) for an event is defined by*

$$u_x = a \sin t$$
$$u_y = b \cos t$$
$$u_z = 0 \ .$$

*Construct a covariance matrix using Equation 6.1 and show that the two nonzero eigenvalues of this matrix are proportional to $a$ and $b$.*

For this problem, the covariance matrix defined by Equation 6.1 can be expressed in continuous form as

$$\mathbf{C} = \begin{bmatrix} \frac{a^2}{T} \int_0^T \sin^2(t)dt & \frac{ab}{T} \int_0^T \sin(t)\cos(t)dt & 0 \\ \frac{ab}{T} \int_0^T \sin(t)\cos(t)dt & \frac{b^2}{T} \int_0^T \cos^2(t)dt & 0 \\ 0 & 0 & 0 \end{bmatrix} .$$

Since:

$$\int \sin^2(t)dt = \tfrac{1}{2}\left(t - \sin(t)/2\right)$$

$$\int \cos^2(t)dt = \tfrac{1}{2}\left(t + \sin(t)/2\right)$$

$$\int \sin(t)\cos(t)dt = \sin^2(t)/2$$

and $T = N\pi$, the covariance matrix reduces to

$$\mathbf{C} = \begin{bmatrix} \frac{a^2}{2} & 0 & 0 \\ 0 & \frac{b^2}{2} & 0 \\ 0 & 0 & 0 \end{bmatrix} .$$

The eigenvalues of this matrix are $\frac{a^2}{2}$, $\frac{b^2}{2}$ and zero. Jurkevics (1988) defines the polarization problem as finding the eigenvalues ($\lambda_1 \lambda_2 \lambda_3$) and eigenvectors ($\mathbf{u_1 u_2 u_3}$) that are nontrivial solutions to

$$(\mathbf{C} - \lambda^2 \mathbf{I})\mathbf{u} = 0,$$

where $\mathbf{I}$ denotes the identity matrix. Comparing this with the matrix above, we see that the polarization is defined by elliptical motion in the $x - y$ plane with axis lengths that are proportional to $a$ and $b$, respectively.

## 6.2 Problem 2

*Consider a time series given by random white noise with a root-mean-squared amplitude of $A_N$ and a unit impulse at $t$ = 0. Draw a sketch of the characteristics functions using STA/LTA, kurtosis and AIC approaches for signal detection.*

See examples given in the online problem below.

## 6.3 Problem 3

*Consider a shale layer that contains thin coal intervals, as defined in Problem 4b of Chapter 1. In addition, the shale density is 2200 kg/m$^3$ and the coal density is 1800 kg/m$^3$. Determine the layer parameters (isotropic $v_P$ and $v_S$, or VTI parameters as appropriate).*

a) *Take the thickness-weighted average of the $v_P$ and $v_S$ of the constituent beds. This is a commonly used approach for blocking velocity models.*

Based on the information given above and in Problem 4b of Chapter 1, the velocities in the shale layer are $v_P = 3.80$ km/s and $v_S = 2.24$ km/s, whereas the velocities in the coal layer are $v_P = 2.11$ km/s and $v_S = 1.05$ km/s, respectively. Problem 4b specifies that coal layers that are 10 percent of the thickness of shale layers, on average. Thus, the thickness weighted average velocities of the medium are $v_P = 3.63$ km/s and $v_S = 2.12$ km/s.

b) *Take the time-weighted average of the $v_P$ and $v_S$ of the constituent beds.*

In this case, the weighted mean of the respective velocities is determined with weights given by $\left(\dfrac{t_{shale}}{t_{shale} + t_{coal}}\right)$ and $\left(\dfrac{t_{coal}}{t_{shale} + t_{coal}}\right)$ for shale and coal, respectively, where $t_{shale}$ is the transit time for a shale layer that is 90 percent of the total thickness. Likewise, $t_{coal}$ is the transit time for a shale layer that is

10 percent of the total thickness. The total thickness is arbitrary. Use of these weights leads to time-weighted average velocities of the medium are $v_P = 3.52$ km/s and $v_S = 2.01$ km/s. In this scheme, the coal layer has a greater weighting as it is slower and the transit time is relatively larger.

c) *Take the time-weighted average of the slownesses (reciprocal of velocity) of the constituent beds.*

The calculation is similar to the previous calculation, except that the reciprocal of the average of the reciprocal velocities is used, leading to $v_P = 3.35$ km/s and $v_S = 1.84$ km/s. This approach is equivalent to the Wyllie time-average equation for well-log data (Wyllie et al., 1956).

d) *Calculate the equivalent VTI medium using Backus averaging (as in Problem 4b). Express your results using Thomsen (1986) parameters of $\alpha, \beta, \gamma, \delta$ and $\epsilon$.*

Using the elastic stiffness matrix components from the solution to Problem 4b of Chapter 1 and Equations 3.35, 3.36, 3.40, 3.41 and 3.45 we find that $\alpha = 3.43$ km/s, $\beta = 1.93$ km/s, $\epsilon = 0.07$, $\gamma = 0.12$ and $\delta = -0.04$.

## 6.4 Problem 4

*Use the Brune spectral method to estimate the magnitude of the event depicted in Figure 6.17, assuming $v_S = 2500$ m/s, $\rho = 2600$ kg/m$^3$ and $r = 500$ m.*

Based on the Brune model, seismic moment ($M_0$) can be determined from the low-frequency plateau amplitude of the displacement spectrum using Equation 3.88. Using an estimated value of $A_0 = 4 \times 10^{-11}$ m-s, this yields $M_0 = 1.62 \times 10^7$ N-m. From Equation 3.81, this corresponds with a moment magnitude of $M_W = -1.2$.

## 6.5 Online Exercise

The objectives of this exercise are:

1 to study the effect of window size in short time average (STA) and long time average (LTA) ratio method, Modified Energy Ratio (MER) method and to explore the Akaike Information Criterion (AIC) method;
2 to perform interactive picking of $P$- and $S$-arrival times on microseismic data.

The basic theory for the methods used in this assignment is discussed by Akram (2014), and is summarized below. The classic short- and long-time average ratio

(STA/LTA) technique is the most widely used approach for event detection and time picking. The first step is to compute moving average values for both a short-time window and a long-time window, as follows:

$$STA(t) = \text{mean}\left\{u\left(t - \tfrac{t_S}{2} \leq t \leq t + \tfrac{t_S}{2}\right)\right\},$$

and

$$LTA(t) = \text{mean}\left\{u\left(t - \tfrac{t_L}{2} \leq t \leq t + \tfrac{t_L}{2}\right)\right\}.$$

In these expressions, $u(t)$ is a seismic trace, and $t_S$ and $t_L$ are the short and long window lengths, respectively. Han et al. (2009) recommended a STA window size that is 2 - 3 times the dominant period of the seismic signal and a LTA window size equal to 5 - 10 times the STA window size. Although these guidelines are reasonable, an LTA window length that is 7 - 12 times the STA window length may yield better results. The STA/LTA ratio is given by

$$R(t) = \frac{STA(t)}{LTA(t)} \; .$$

The MER algorithm, proposed by Han et al. (2009), differs from the STA/LTA algorithm in the sense that it uses both pre- and post-sample windows of equal size for energy ratio calculations. Consider an energy ratio (ER) given by

$$ER_i = \frac{\sum_{j=i}^{i+w} u_j^2}{\sum_{j=i-w}^{i} u_j^2} \; ,$$

where $w$ is the window length. The modified energy ratio (MER) is given by

$$MER_i = |u_i|^3 ER_i \; .$$

The AIC algorithm is based on the idea that non-stationary characteristics of microseismic signals can be approximated by dividing an observed trace into locally stationary segments, where each is treated as an autoregressive process. For a trace of length $N$, the AIC characteristic curve is represented as

$$AIC_k = k \log\left(\text{var}\left\{u_{i:k}\right\}\right) + (N - k + 1)\log\left(\text{var}\left\{u_{k+1:N}\right\}\right) \; ,$$

where $k$ ranges through all samples of the input microseismic trace. A local minimum value of the AIC characteristic curve represents the arrival time. Unlike STA/LTA and MER, this technique does not require the selection of a window size.

### 6.5.1 Procedure

1. Test parameters for STA/LTA using the program STA_LTA_tool. After selecting a dataset for processing, this program runs through each trace. Select the approximate start time and threshold value in the STA/LTA window using the mouse. As illustrated below, the algorithm will "snap" to the next peak in the normalized STA/LTA characteristic curve. Once completed, the 3-component record section is plotted with your picks indicated by green arrows.

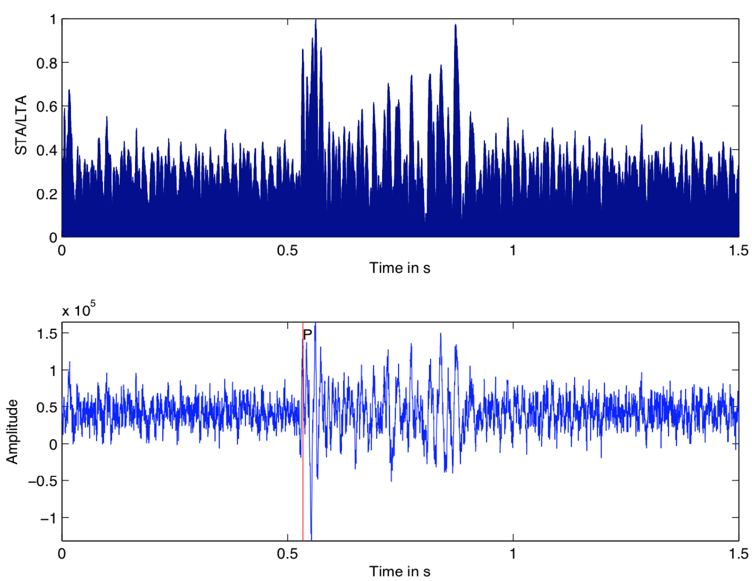


2. Test the window length for the Maximum Energy Ratio (MER) method using the program MER_tool. The program works in much the same way as STA_LTA_tool, except that the MER characteristic curve is shown with a logarithmic scale as illustrated below.

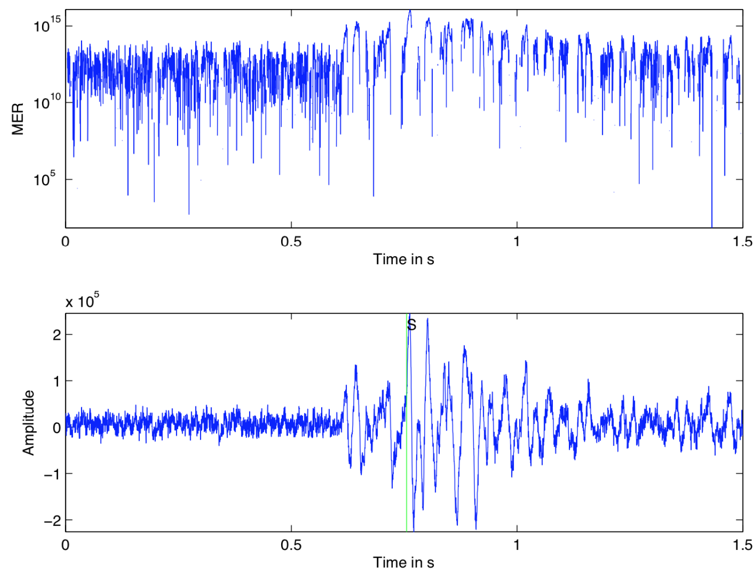


3. Use the program AIC_tool to pick $P$- and $S$-wave arrival times. This program works in a similar manner to the previous ones, but in this case pick just above and prior to the appropriate local minimum in the AIC characteristic curve.

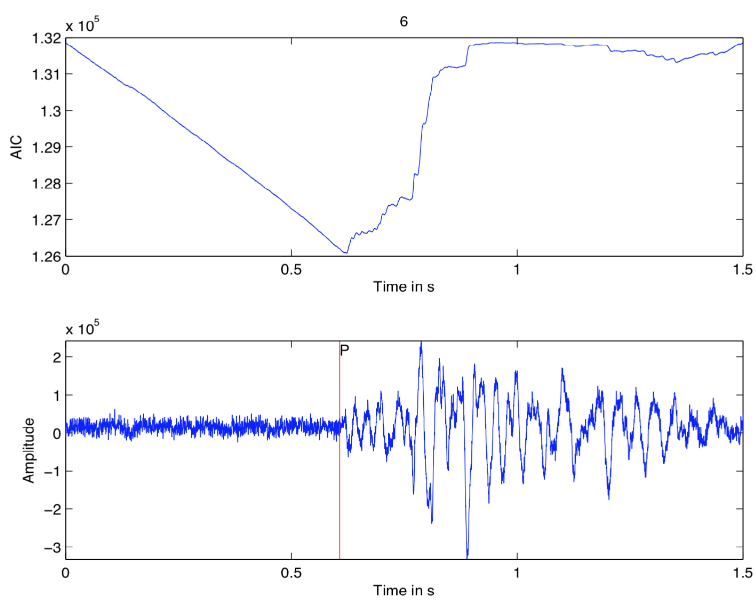


For all three of the programs described above, when finished picking you will see a record section with the picks marked by green plus symbols as illustrated below. Zoom in to examine the picks in detail.

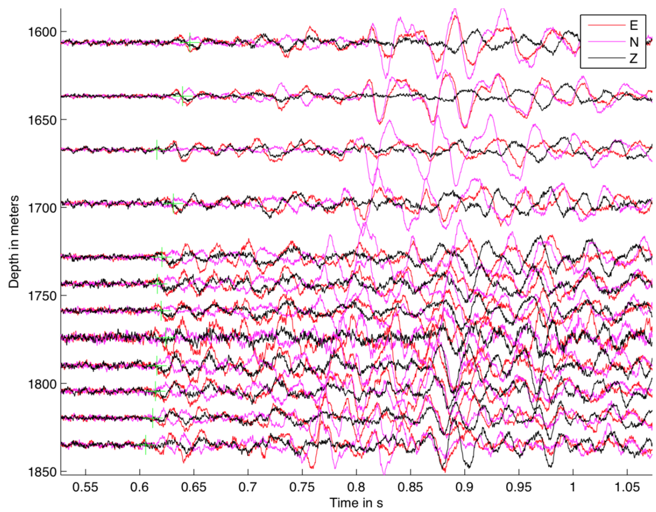


4. Compare the automatically picked first arrival times using STA/LTA, MER and AIC methods. The goal is to optimize the parameters to pick the $P$-wave first arrival accurately for the events.

# 7 Chapter 7

## 7.1 Problem 1

*Raw microseismic data requires conversion into units of velocity. If the background noise falls within the range of $\pm$ 0.2 raw amplitude units, what is the corresponding range of displacement in m/s, given a sensitivity of $S_i$ = 85.8 V/m/s and an amplifier gain of $g_a$ = 72 dB?*

From Equation 7.7, the correction term is given by $\xi_c = S_i\, 10^{g_a/20}$. Based on the information provided above, $\xi_c = 3.42 \times 10^5$. Hence, the background noise is in the range of 5.86 $\times 10^{-7}$ m/s.

## 7.2 Problem 2

*Consider the shallow borehole station depicted in Figure 7.2a. Given the known depths, determine the near-surface P-wave velocity, given the arrival times of 2.451, 2.455, 2.459 s for the three 1C components (from the top), and 2.465 s for the 3C receiver at the bottom. What is the near-surface velocity? Does this value fall into the range of expected near-surface P-wave velocity?*

By simply using the depths (12 m and 27 m) and times for the shallowest and deepest geophone levels, the estimated apparent velocity is $v_P \simeq 1071$ m/s. If linear regression is used, then the estimated apparent velocity is $v_P \simeq 1087$ m/s. This velocity falls within the expected range for dry sand.

## 7.3 Problem 3

*Consider the shallow buried array in Figure 7.7. If hydraulic fracturing is performed at a depth of 3.0 km in the eastern horizontal well and 3C geophones are used to record the resulting microseismic events, on which components do you expect to record the P-wave, and on which do you expect to record the S-wave? Next, consider an event originating at depth outside the limits of the array to the northwest. On which components would you then expect to see the dominant P- and S-wave* *motion? Assume that the $v_P$ and $v_S$ of the near-surface unconsolidated layer is much less than the velocities in the underlying layers.*

The presence of low-velocity overburden means that both $P$ and $S$ waves are expected to refract into near-vertical incidence at the surface. Consequently, the $P$ wave for a microseismic source location near the east well at 3.0 km depth will be recorded primarily on the vertical-component geophones. For a source located northwest of the array, some horizontal ground motion is also expected, along a northwest - southeast azimuth. $S$ waves will tend to be recorded on horizontal geophone components irrespective of the source location. The relationship of the $S$-wave polarization to the source position is more complex.

## 7.4 Problem 4

*Sketch the wavefronts for both cases in Problem 3. How would you characterize the moveout that would be expected for both events, if the receivers were re-ordered by distance from the central well?*

To a first approximation, wavefronts for a source 3 km below the geophone array would be propagating vertically upwards. On the other hand, wavefronts for a source that is located northwest of the array, wavefronts would propagate toward the SE with oblique incidence at the surface. In the former case, the moveout would be approximately hyperbolic with distance from the central well; in the latter case, the moveout would have a more complex pattern.

# 8 Chapter 8

## 8.1 Problem 1

*The table below summarizes the number events within magnitude bins of width one magnitude unit and centred at values shown by $M$. Suppose that these events were detected within the same study area, during three different time windows of varying length.*

| $M$ | 1 day | 7 days | 28 days |
|---|---|---|---|
| 0 | 48 | 346 | 1329 |
| 1 | 4 | 28 | 110 |
| 2 | 0 | 2 | 9 |
| 3 | 0 | 0 | 1 |

a) *Estimate the b-value by linear regression. Assume that the table is complete to the lowest magnitude bin.*

Linear regression with the values tabulated above yields $b$-values of 1.08, 1.12 and 1.05, respectively.

b) *Based on this simple example, how many observations do you think are necessary for reliable determination of b-value?*

Clearly, uncertainties in determination of $b$-value are reduced when using a larger catalog (assuming a stationary process). An issue for the toy example considered here is the use of large magnitude bins. For a discussion of a robust approach for determining maximum-likelihood $b$-value with grouped magnitude values, the reader is referred to Bender (1983).

## 8.2 Problem 2

.
*The table below shows the locations for 10 coplanar events. Locations denoted by $(x', y', z')$ contain noise, whereas those denoted by $(x, y, z)$ are noise-free. Using*

*equation 8.2, calculate the $D$ value for both of these sets of events. What does this tell you about the effects of location uncertainty on the calculated $D$ value?*

| $x$ | $y$ | $z$ | $x'$ | $y'$ | $z'$ |
|---|---|---|---|---|---|
| 162 | 451 | 759 | 158 | 465 | 919 |
| 794 | 84 | 525 | 772 | 78 | 613 |
| 311 | 229 | 502 | 331 | 216 | 309 |
| 529 | 913 | 1637 | 551 | 909 | 1928 |
| 166 | 152 | 314 | 165 | 132 | 588 |
| 602 | 826 | 1542 | 601 | 807 | 1741 |
| 263 | 538 | 941 | 255 | 560 | 852 |
| 654 | 996 | 1824 | 674 | 1019 | 1685 |
| 689 | 78 | 464 | 683 | 82 | 376 |
| 748 | 443 | 1041 | 729 | 421 | 1070 |

The fractal dimension ($D$) can be estimated using Equations 8.2 and 8.3. Numerical estimation using the discrete set of values of distance ($r$) given by [200,300,400,500,600,700,800,900,1000] yields a $D$ value of 1.68 for the noise-free data and 1.93 for the noisy data. Recall that, since the points are coplanar, the expected fractal dimension is 2.0. The inferred fractal dimension is lower because of the limited spatial extent of the data. The addition of noise, which makes the point cloud more diffuse, has the effect of increasing $D$.

## 8.3 Problem 3

*Supplementary Table 1 in the online materials contains locations, times and magnitudes for a series of events that could be classified variously into clusters. Discuss various approaches that could be used to cluster these events.*

The reader is referred to Jain et al. (1999) for a comprehensive review of different clustering techniques, many of which are implement in Matlab.

## 8.4 Problem 4

*For the tabulated events in question 3:*

a) *make an $r - t$ graph to determine the apparent diffusivity;*
b) *evaluate attributes listed in Table 8.2.*

The $x - y$ position of the microseismic events from Supplementary Table 1 are plotted below. The events are grouped into three stages as marked. Given the limited amount of data available in the Supplementary Table, not all of the attributes in Table 8.2 can be computed. Examples of attributes that can be determined include cluster length, height, azimuth and duration; mean magnitude and magnitude variance; $b$ value and $D$ value; net seismic moment; maximum-moment rate; and seismic-moment density.

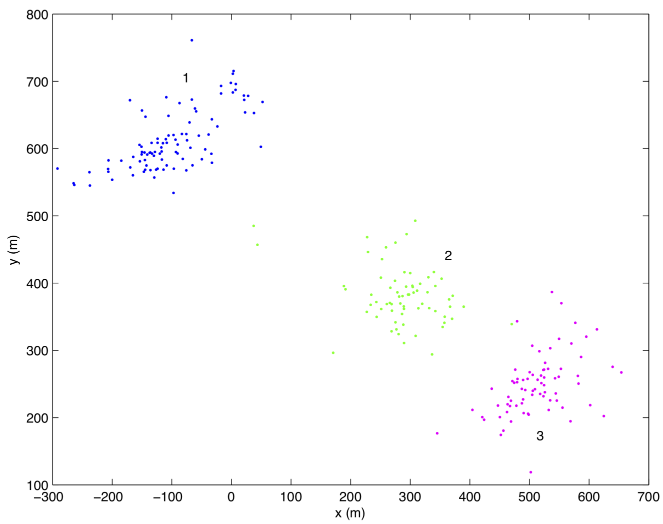


The following diagram shows and $r-t$ graph, including events from all three of the stages in the Supplementary Table. A set of curves with varying values of apparent diffusivity are plotted, with $D =$, 10, 5, 2 and 1 m$^2$/s, respectively.

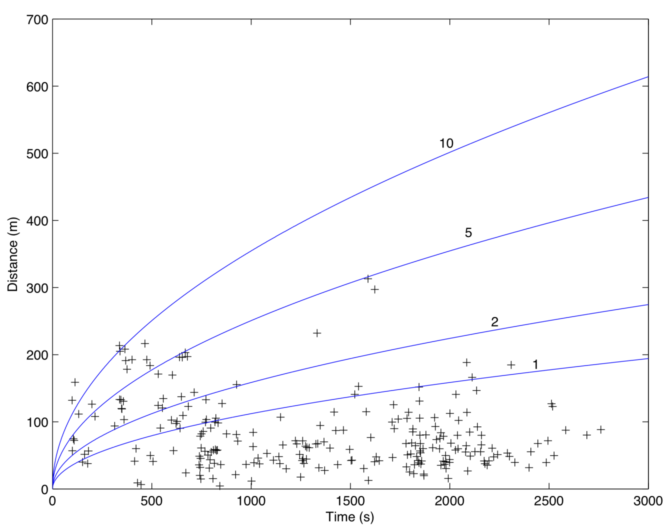

## 8.5 Problem 5

*Use Equation 8.7 to determine the most-positive curvature corresponding to the following analytically defined surfaces.*

a) *A sphere of radius $a$.*
b) *A paraboloid defined by $z = x^2/a^2 + y^2/b^2$.*

At any point on a curved surface there are two principal curvatures, the maximum curvature, $\kappa_1$, and minimum curvature, $\kappa_2$. The product of these is the Gaussian curvature, $k_{Gauss} = \kappa_1\kappa_2$ and the average is the mean curvature, $k_{mean} = \frac{\kappa_1+\kappa_2}{2}$. For a sphere of radius $a$, we have $\kappa_1 = 1/a$ and $\kappa_2 = 1/a$, so $k_{Gauss} = 1/a^2$ and $k_{mean} = 1/a$. Substituting these values into Equation 8.7 yields $k_1 = k_{mean} = 1/a$.

To make the calculation for a paraboloid, we can use Equations 8.4 - 8.7. Comparing the formula for the paraboloid surface defined above with Equation 8.4, we see that the coefficients $c, d, e$ and $f$ in Equation 8.4 are all zero. From Equation 8.6, this gives $k_{Gauss} = \frac{4}{a^2b^2}$. From Equation 8.5, this gives $k_{mean} = \frac{1}{a^2} + \frac{1}{b^2}$. Substitution into Equation 8.7 shows that $k_1 = \frac{2}{a^2}$ $(a \leq b)$ or $k_1 = \frac{2}{b^2}$ (otherwise).

## 8.6 Online Exercise

In this exercise, the convex-hull method described in Box 8.1 is used to calculated Estimated Stimulated Volume (ESV) using the three sample microseismic clusters from Problems 3 and 4. The basic methodology is outlined in Figures 8.7 and 8.8.

### 8.6.1 Procedure

The program used in this exercise is called ESV_tool. When the program is invoked, the user is asked to select the sample dataset. For convenience, these are stored under file names cluster1.mat, cluster2.mat and cluster3.mat in the Chapter8 folder. These files contain the event location information from Supplementary Table 1, as well as the location of the injection point and a reported location uncertainty. This dataset is from downhole microseismic monitoring of a tight sand reservoir in central Alberta, Canada. The location uncertainties reflect standard errors in location determined from the picking uncertainties, and do not include other sources of error such as uncertainties in the velocity model.

As illustrated in Figure 8.8, ESV_tool calculates the upper and lower of the estimated stimulated volume using the convex-hull approach together with the reported uncertainty data.

# 9 Chapter 9

## 9.1 Problem 1

*Calculate the seismogenic index (Equation 9.1) for cluster 1 and well pad 1 using supplementary data from Bao and Eaton (2016), assuming a b-value of unity. The data are freely available in Tables S5 and S7, respectively, at:*

http://science.sciencemag.org/content/suppl/2016/11/16/science.aag2583.DC1

Based on seismicity and fluid injection data, the caclulated seismogenic index reported by Bao and Eaton (2016) in their supplementary data table S4 are $-2.7$, $-1.7$, $-1.5$ and $-1.5$ for clusters 1, 2, 3 and 6, respectively.

## 9.2 Problem 2

*Calculate the pore-pressure increase caused by a point source with a constant flux within a homogeneous poroelastic medium (Equation 9.2), using the following parameters: flux rate $q/\rho_0 = 10^{-2}$ $m^3/s$, dynamic viscosity $\eta$ = $10^{-3}$ Pa-s, permeability $\kappa$ = $10^{-15}$ $m^2$ and hydraulic diffusivity $c$ = 0.1 $m^2/s$. Calculate the pore pressure at distances of $r$ = 500 m and 5.0 km and injection times of 30 days and 1 year. Be mindful of units.*

From Equation 9.2, at a distance of 500 m these parameters give $P = 0.8$ MPa after 30 days and $P = 1.3$ MPa after one year (365 days). Similarly, at a distance of 5.0 km these parameters give $P \approx 0$ after 30 days and $P = 7.4$ kPa after one year.

## 9.3 Problem 3

*Based on the seismicity and injection data for cluster 1 from question 1, determine and compare the maximum magnitude obtained using the method of McGarr (2014) and the method of Van der Elst et al. (2016), as described in Box 9.1.*

According to McGarr (2014), the maximum seismic moment is given by $M_0 = \mu \Delta V$, where $\Delta V$ is the net injected volume. Using the data from Problem 1($\Delta V$ = 59.6 $\times$ $10^3$ $m^3$, $\Delta V$ = 120.4 $\times$ $10^3$ $m^3$, $\Delta V$ = 26.8 $\times$ $10^3$ $m^3$ and $\Delta V$ = 37.4 $\times$ $10^3$ $m^3$) with $\mu = 3 \times 10^{10}$ Pa, the predicted maximum magnitudes are 4.2, 4.4, 3.9 and 4.0 for clusters, 2, 3 and 6, respectively.

According to Van der Elst et al. (2016) the maximum magnitude for fluid injection can be written as $\frac{1}{b}(\Sigma + \log_{10} V)$, where $\Sigma$ is the seismogenic index. Using the seismogenic indices from Problem 1 and assuming $b = 1$, the predicted maximum magnitudes are 2.1, 3.4, 2.9 and 3.1 for the same set of clusters.

Bao and Eaton (2016) reported an event of magnitude $M_W$ 3.9 for cluster 1 from this dataset.

## 9.4 Problem 4

*Suppose that there are two seismogenic source regions at distances of 20 km and 200 km from a particular area of interest. The near region is characterized by annual Gutenberg-Richter parameters of $a$ = 5.2 and $b$ = 1.2, while the farther region has $a$ = 4.1 and $b$ = 0.9.*

a) *Using the ground-motion prediction equation (GMPE) given in equation 5.11 with parameters for eastern North America from Atkinson et al. (2014), calculate the pseudoacceleration amplitude (in cm/$s^2$) for both distance ranges, for a period of 0.3 s and a magnitude of M4.*

Equation 5.11 is a GMPE that expresses pseudoacceleration amplitude as a function of magnitude and distance. At a period of 0.3 s, the coefficients for eastern North America are $C_T = -3.3$ and $\gamma_T$ =0.0015. Combined with the distance relationship in Equation 5.12, the calculated values are PSA = 6.0 cm/$s^2$ and 0.5 cm/$s^2$ at distances of 20 km and 200 km. Note the differing forms of the geometrical attenuation in Equation 5.12 for these two distance ranges.

b) *Calculate the expected number of M4, M6 and M8 events in both regions, in a 50-year time interval.*

Based on the Gutenberg-Richter formula with the parameters given, the expected number of events in a 50-year period (rounded to the nearest integer) are 126 and 1 in the case of the near region with $a$ = 5.2 and $b$ = 1.2, for M4 and M6, respectively. The expected number of events in a 50-year period for the farther region with $a$ = 4.1 and $b$ = 0.9 are 158 and 3 for M4 and M6 respectively. Based on the parameters given, the probability of a M8 event in either area is small.

## 9.5 Online Exercise

A review of seismicity, structure, tectonics, volcanism, earthquake triggering mechanisms, and gas geochemistry in West Bohemia and the adjacent Vogtland region is presented by Fischer et al. (2014). The most active part of this region contains three Quaternary active volcanoes and coincides with the intersection of the Eger Rift and RegensburgLeipzigRostock Zone. The latitude-longitude range for the seismically active area is approximated by 50° - 50.5° N and 12° - 12.7°E.

There are many websites that provide tools for downloading earthquake data. A useful compilation of sites (especially in North America) can be found at:

www.geophysics.geol.uoa.gr/frame_en/insti/seisurf.html

The Observatories and Research Facilities for European Seismology (ORFEUS) site provides access to digital waveform data and station metadata through the European Integrated Data Archive:

https://www.orfeus-eu.org/data/eida/

This service allows a user to specify a latitude-longitude window, query available stations and data. The data can be downloaded in Mini SEED or Full SEED format, while various formats exist for metadata. Similarly, the Incorporated Research Institutes in Seismology (IRIS) provides a variety of tools to access online data from global seismograph networks:

http://ds.iris.edu/ds/nodes/dmc/tools/

# References

Akram, J. 2014. *Downhole microseismic monitoring: processing, algorithms and error analysis*. Ph.D. thesis, University of Calgary.

Atkinson, G.M., Greig, D.W., and Yenier, E. 2014. Estimation of moment magnitude (M) for small events (M $<$ 4) on local networks. *Seismological Research Letters*, **85**(5), 1116–1124.

Bao, X., and Eaton, D.W. 2016. Fault activation by hydraulic fracturing in western Canada. *Science*, **354**(6318), 1406–1409.

Bender, Bernice. 1983. Maximum likelihood estimation of b values for magnitude grouped data. *Bulletin of the Seismological Society of America*, **73**(3), 831–851.

Courtney, E.C. 2000. *The Mechanical Behavior of Materials*. Waveland Press.

Fischer, T., Horálek, J., Hrubcová, P., Vavryčuk, V., Bräuer, K., and Kämpf, H. 2014. Intra-continental earthquake swarms in West-Bohemia and Vogtland: a review. *Tectonophysics*, **611**, 1–27.

Han, L, Wong, J, Bancroft, J, et al. 2009. Time picking and random noise reduction on microseismic data. *CREWES Research Report*, **21**, 1–13.

Hudson, J.A., Pearce, R.G., and Rogers, R.M. 1989. Source type plot for inversion of the moment tensor. *Journal of Geophysical Research: Solid Earth*, **94**(B1), 765–774.

Jain, A.K., Murty, M.N., and Flynn, P.J. 1999. Data clustering: A review. *ACM computing surveys (CSUR)*, **31**(3), 264–323.

Jurkevics, A. 1988. Polarization analysis of three-component array data. *Bulletin of the Seismological Society of America*, **78**(5), 1725–1743.

King, G.C.P., Stein, R.S, and Lin, J. 1994. Static stress changes and the triggering of earthquakes. *Bulletin of the Seismological Society of America*, **84**(3), 935–953.

Langenbruch, Cornelius, and Shapiro, Serge A. 2010. Decay rate of fluid-induced seismicity after termination of reservoir stimulations. *Geophysics*, **75**(6), MA53–MA62.

Lin, Jian, and Stein, Ross S. 2004. Stress triggering in thrust and subduction earthquakes and stress interaction between the southern San Andreas and nearby thrust and strike-slip faults. *Journal of Geophysical Research: Solid Earth*, **109**(B2).

McGarr, A. 2014. Maximum magnitude earthquakes induced by fluid injection. *Journal of Geophysical Research: Solid Earth*, **119**(2), 1008–1019.

Thomsen, L. 1986. Weak elastic anisotropy. *Geophysics*, **51**(10), 1954–1966.

Toda, Shinji, Stein, Ross S, Richards-Dinger, Keith, and Bozkurt, Serkan B. 2005. Forecasting the evolution of seismicity in southern California: Animations built on earthquake stress transfer. *Journal of Geophysical Research: Solid Earth*, **110**(B5).

Van der Elst, N.J., Page, M.T., Weiser, D.A., Goebel, T.H.W., and Hosseini, S.M. 2016. Induced earthquake magnitudes are as large as (statistically) expected. *Journal of Geophysical Research: Solid Earth*, **121**(6), 4575–4590.

Wyllie, Malcolm Robert Jesse, Gregory, Alvin Ray, and Gardner, Louis Wright. 1956. Elastic wave velocities in heterogeneous and porous media. *Geophysics*, **21**(1), 41–70.